Electronic Supplementary Material (ESI) for Journal of Materials Chemistry A.

Supplementary Information

In-situ inserting shutter ions in MnO_2 to boost supercapacitive performance of flexible supercapacitor

Haoyu Wei, Tongchuan Sun, Mingyue Liu, Qingyang Pang, Yuting Qian, Xinwen Dou, Yuwei Zhang, Qiang Ju* and Zhenlan Fang*

School of Flexible Electronics (Future Technologies) & Institute of Advanced Materials (IAM), Key Laboratory of Flexible Electronics (KLOFE), Jiangsu National Synergetic Innovation Center for Advanced Materials (SICAM), Nanjing Tech University (NanjingTech), Nanjing 211816 (China). Email: iamqju@njtech.edu.cn; iamzlfang@njtech.edu.cn

Table of Contents

1.0 The components of δ-($M^{+}{}_{y}Mn^{3+}{}_{y}Mn^{4+}{}_{1-y}$)$O^{2-}{}_{2}$@ACC

Tab. 1 The components of δ-($M^{+}{}_{y}Mn^{3+}{}_{y}Mn^{4+}{}_{1-y}$)$O^{2-}{}_{2}$@ACC.

Sample Names	y^{a}	y^{b}
δ-($Li^{+}{}_{y}Mn^{3+}{}_{y}Mn^{4+}{}_{1-y}$)$O^{2-}{}_{2}$@ACC	0.41	0.40
δ-($Na^{+}{}_{y}Mn^{3+}{}_{y}Mn^{4+}{}_{1-y}$)$O^{2-}{}_{2}$@ACC	0.49	0.48
δ-($K^{+}{}_{y}Mn^{3+}{}_{y}Mn^{4+}{}_{1-y}$)$O^{2-}{}_{2}$@ACC	0.54	0.55

[a]The y values determined by XPS analysis (Mn 2$p_{3/2}$ spectra).[1]
[b]The y values determined by XPS analysis (O 1*s* spectra).

2.0 Electrochemical performance of δ-$(Na^{+}_{y}Mn^{3+}_{y}Mn^{4+}_{1-y})O^{2-}_{2}$@ACC

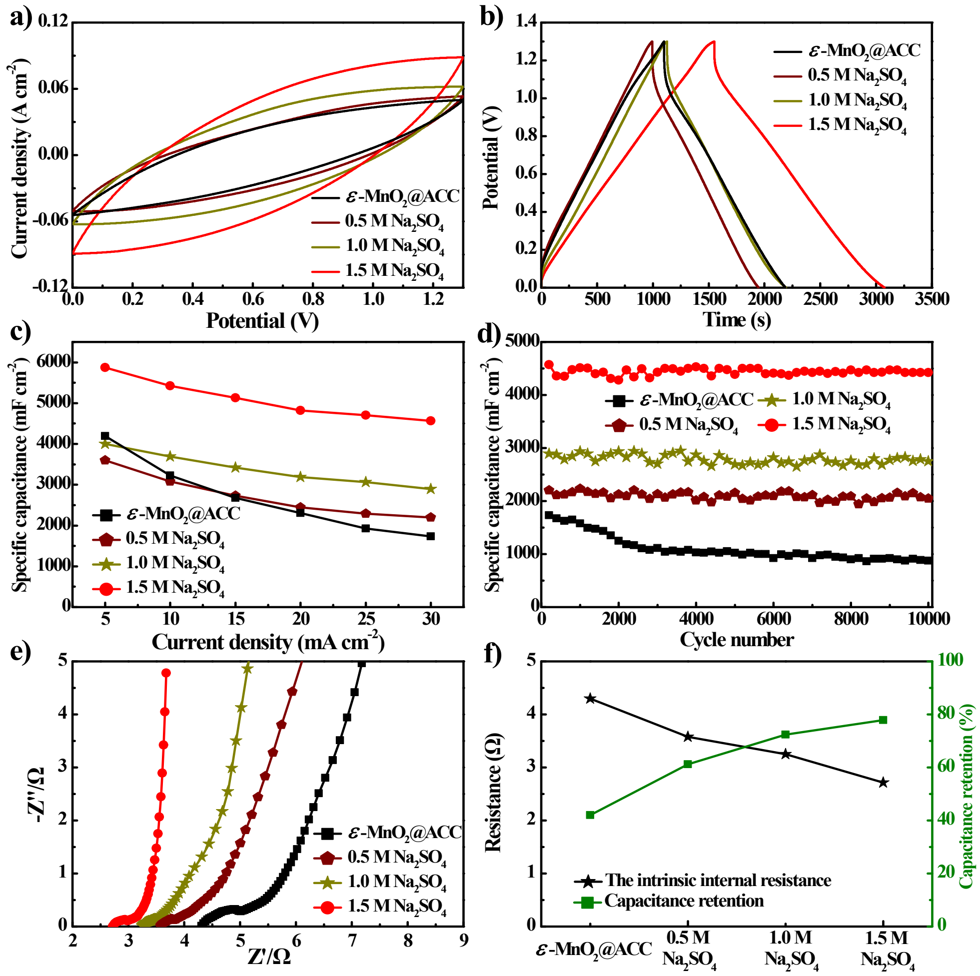

Supplementary Fig. 1 Electrochemical performances of a series of δ-$(Na^{+}_{y}Mn^{3+}_{y}Mn^{4+}_{1-y})O^{2-}_{2}$@ACC, in which Na^{+} was inserted by CV sweep at Na_2SO_4 electrolyte with varied concentration of 0.5 M, 1.0 M, and 1.5 M, respectively, for 500 times: (a) CV curves at 20 mV s^{-1}, (b) GCD curves at 5 mA cm^{-2}, (c) the areal capacitances at various discharge current densities ranging from 5 to 30 mA cm^{-2}, (d) the plots of areal capacitance at 30 mA cm^{-2} over 10,000 charge/discharge cycles, (e) Nyquist plots, (f) the resistance and the capacitance retention upon increasing the discharge current density from 5 to 30 mA cm^{-2}. Note: δ-$(Na^{+}_{y}Mn^{3+}_{y}Mn^{4+}_{1-y})O^{2-}_{2}$@ACC and ε-MnO_2@ACC tested in 1.5 M Na_2SO_4.

To ascertain the optimal electrolyte concentration for fabricating δ-$(Na^{+}_{y}Mn^{3+}_{y}Mn^{4+}_{1-y})O^{2-}_{2}$ *in-situ* growing on activated carbon cloth (ACC) [δ-$(Na^{+}_{y}Mn^{3+}_{y}Mn^{4+}_{1-y})O^{2-}_{2}$@ACC] electrode by electrochemical method, the electrochemical performances of a series of δ-$(Na^{+}_{y}Mn^{3+}_{y}Mn^{4+}_{1-y})O^{2-}_{2}$@ACC electrodes, in which Na^{+} ions were inserted by CV sweep in 0.5 M Na_2SO_4, 1.0 M Na_2SO_4, and 1.5 M Na_2SO_4, respectively, for 500 times, were tested under the same condition of ε-

MnO_2@ACC. The CV curves at 20 mV s^{-1} of these electrodes were highly similar, demonstrating that the charge storage process of them includes both the surface capacitive and the diffusion-controlled processes (Supplementary Fig. 1a). The areal capacitances (Supplementary Fig. 1c) are determined from the GCD curves (Supplementary Fig. 1b), while the rate capabilities (Supplementary Fig. 1f) are calculated based on the capacitance retentions upon increasing the discharge current density from 5 to 30 mA cm^{-2} (Supplementary Fig. 1c).

Upon increasing electrolyte concentration for *in-situ* inserting Na^+ shutter ions from 0.5 to 1.5 M, the areal capacitances at the current density 5 mA cm^{-2} of δ-$(Na^+_yMn^{3+}_yMn^{4+}_{1-y})O^{2-}_2$@ACC electrodes are elevated from 3595 to 5875 mF cm^{-2}, and the rate capabilities are boosted from 61.20% to 77.8%, respectively. Moreover, the capacitance retentions of δ-$(Na^+_yMn^{3+}_yMn^{4+}_{1-y})O^{2-}_2$@ACC after charge/discharge at 30 mA cm^{-2} of 10,000 cycles increase from 93% to 97%, much higher than that of ε-MnO_2@ACC (51%, Supplementary Fig. 1d). The R_s values of δ-$(Na^+_yMn^{3+}_yMn^{4+}_{1-y})O^{2-}_2$@ACC stepwise decrease from 3.58 to 2.72 Ω, which are lower than that of ε-MnO_2@ACC (4.30 Ω) (Supplementary Fig. 1e-f). These results illuminate that the optimal electrolyte concentration for *in-situ* inserting Na^+ shutter ions into ε-MnO_2@ACC is 1.5 M Na_2SO_4, which can significantly boost areal capacitance, cycle stability and rate capability, accompanied with slightly decreased R_s value.

3.0 PXRD patterns of δ-$(Na^{+}_{0.48}Mn^{3+}_{0.48}Mn^{4+}_{0.52})O^{2-}_{2}$@ACC

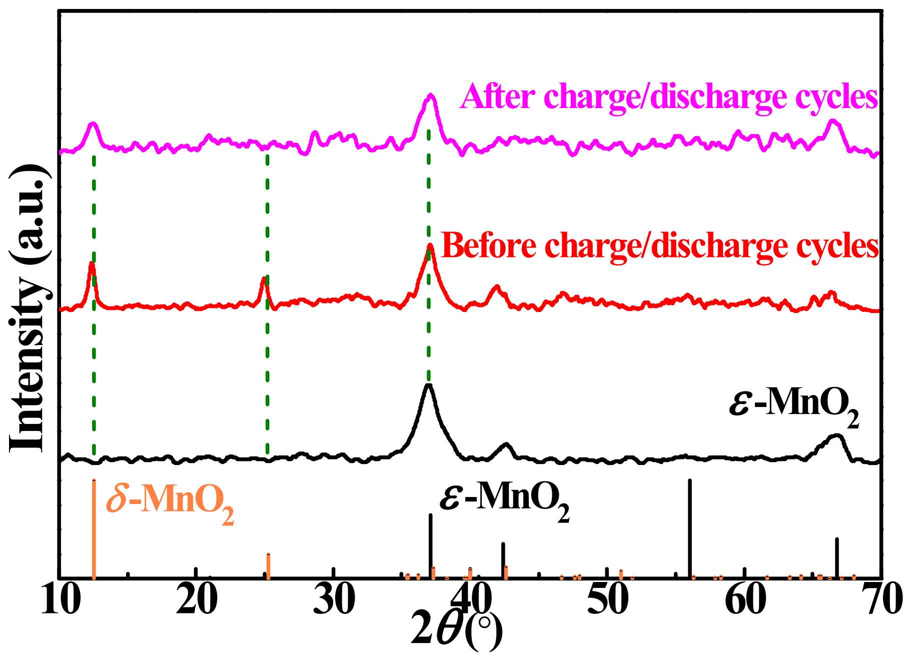

Supplementary Fig. 2 The measured PXRD patterns of ε-MnO_2@ACC and δ-$(Na^{+}_{0.48}Mn^{3+}_{0.48}Mn^{4+}_{0.52})O^{2-}_{2}$@ACC and electrodes before and after 10,000 charge/discharge cycles at a current density of 30 mA cm^{-2} and the PXRD patterns of ε-MnO_2 (PDF # 30-0820) and δ-MnO_2 (PDF # 80-1098) obtained from the powder diffraction file (PDF). Note: the interference peaks from the ACC are subtracted in all measured PXRD for clarity.

To investigate the adhesion of MnO_2 on ACC after long term cycling, take δ-$(Na^{+}_{0.48}Mn^{3+}_{0.48}Mn^{4+}_{0.52})O^{2-}_{2}$@ACC as an example, the PXRD pattern of δ-$(Na^{+}_{0.48}Mn^{3+}_{0.48}Mn^{4+}_{0.52})O^{2-}_{2}$@ACC electrode after 10,000 cycles is indexed to the mixture of ε-MnO_2 and δ-MnO_2, illuminating that MnO_2 has high stability and strong adhesion with ACC (Supplementary Fig. 2).

4.0 Na 1*s* XPS spectra of the selected samples

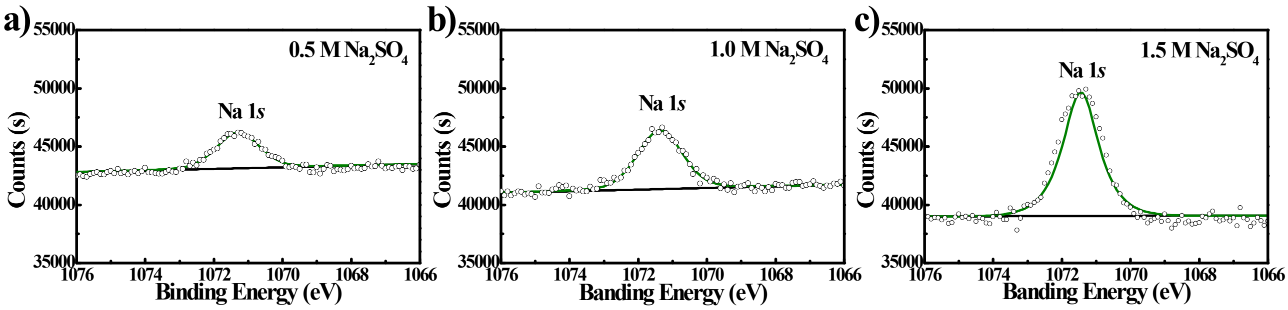

Supplementary Fig. 3 High resolution XPS spectra of Na 1*s* region for a series of δ-($Na^{+}{}_{y}Mn^{3+}{}_{y}Mn^{4+}{}_{1-y}$)$O^{2-}{}_{2}$@ACC, in which Na^{+} was inserted by CV sweep at electrolyte concentration of (a) 0.5 M Na_2SO_4, (b) 1.0 M Na_2SO_4, and (c) 1.5 M Na_2SO_4, respectively, for 500 times.

Tab. 2 The integral area of the Na 1*s* peak of the δ-($Na^{+}{}_{y}Mn^{3+}{}_{y}Mn^{4+}{}_{1-y}$)$O^{2-}{}_{2}$@ACC electrode synthesized in different concentrations of electrolyte.

Electrolyte Concentration	Integral Area
0.5 M Na_2SO_4	5203
1.0 M Na_2SO_4	8893
1.5 M Na_2SO_4	15529

To clarify that the areal capacitance of δ-($Na^{+}{}_{y}Mn^{3+}{}_{y}Mn^{4+}{}_{1-y}$)$O^{2-}{}_{2}$@ACC electrode increases with the increase of electrolyte concentration, the Na 1*s* XPS core spectra of synthesized samples in different electrolyte concentrations have been measured (Supplementary Fig. 3a-c). The integral area of the Na 1*s* peak gradually increase along with the increase of the electrolyte concentration used for insertion of Na^{+} into ε-MnO_2@ACC by CV sweep (Tab. 2), indicating that the content of Na^{+} in the δ-($Na^{+}{}_{y}Mn^{3+}{}_{y}Mn^{4+}{}_{1-y}$)$O^{2-}{}_{2}$@ACC electrode gradually increase along with increasing the electrolyte concentration.[2] Consequently, the largest specific capacitance of the δ-($Na^{+}{}_{y}Mn^{3+}{}_{y}Mn^{4+}{}_{1-y}$)$O^{2-}{}_{2}$@ACC, prepared by CV sweep of ε-MnO_2@ACC for 500 cycles in 1.5 M Na_2SO_4, can be assigned to the highest content of Na^{+} inserted in the δ-($Na^{+}{}_{y}Mn^{3+}{}_{y}Mn^{4+}{}_{1-y}$)$O^{2-}{}_{2}$@ACC electrode.

5.0 Electrochemical performance of δ-($Li^+{}_yMn^{3+}{}_yMn^{4+}{}_{1-y}$)$O^{2-}{}_2$@ACC

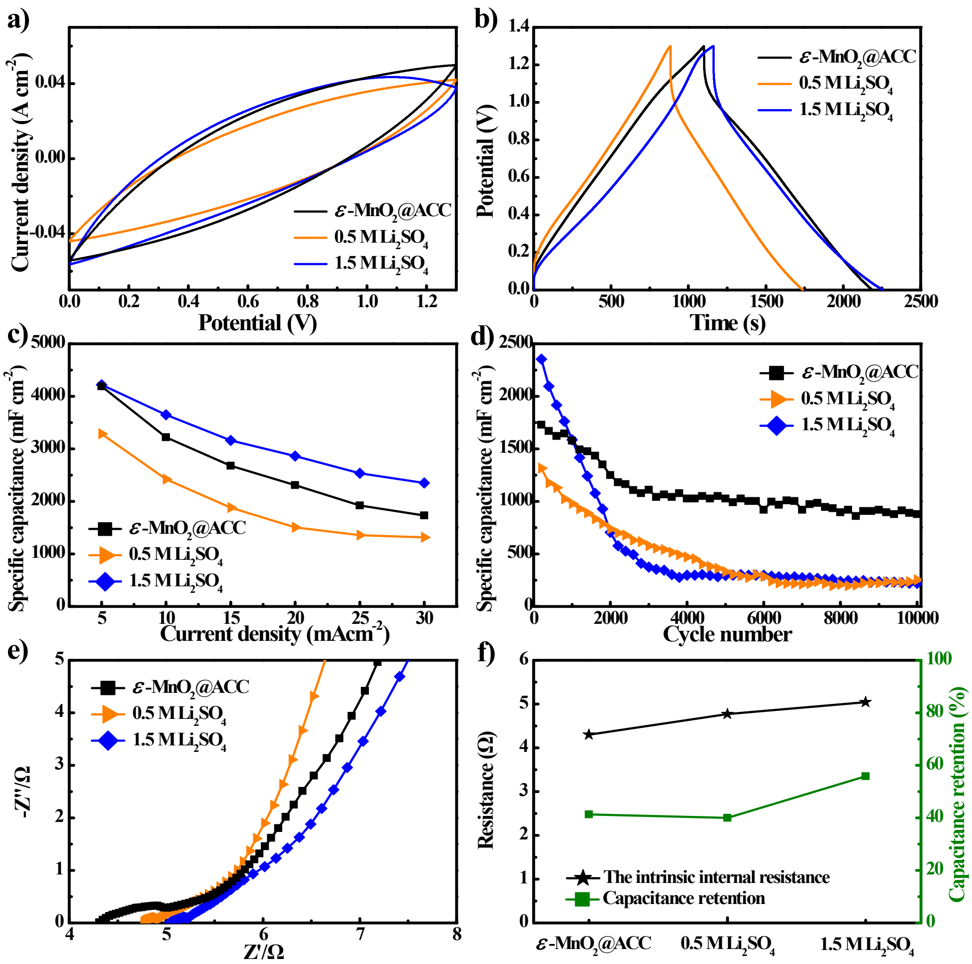

Supplementary Fig. 4 Electrochemical performances of a series of δ-($Li^+{}_yMn^{3+}{}_yMn^{4+}{}_{1-y}$)$O^{2-}{}_2$@ACC, in which Li^+ were inserted by CV sweep at Li_2SO_4 electrolyte with varied concentration of 0.5 M and 1.5 M, respectively, for 500 times, respectively: (a) CV curves at a scan rate of 20 mV s^{-1}, (b) GCD curves at 5 mA cm^{-2}, (c) the areal capacitances at various discharge current densities ranging from 5 to 30 mA cm^{-2}, (d) the plots of areal capacitance at 30 mA cm^{-2} over 10,000 charge/discharge cycles, (e) Nyquist plots, (f) the resistance and the capacitance retention upon increasing the discharge current density from 5 to 30 mA cm^{-2}. Note: δ-($Li^+{}_yMn^{3+}{}_yMn^{4+}{}_{1-y}$)$O^{2-}{}_2$@ACC and ε-MnO_2@ACC tested in 1.5 M Li_2SO_4 and 1.5 M Na_2SO_4, respectively.

To ascertain the optimal electrolyte concentration for fabricating δ-($Li^+{}_yMn^{3+}{}_yMn^{4+}{}_{1-y}$)$O^{2-}{}_2$ electrodes by electrochemical method, the electrochemical performances of two δ-($Li^+{}_yMn^{3+}{}_yMn^{4+}{}_{1-y}$)$O^{2-}{}_2$@ACC electrode in which Li^+ was inserted by CV sweep in 0.5 M Li_2SO_4 and 1.5 M Li_2SO_4, respectively, were tested under the same condition of ε-MnO_2@ACC. The CV curves at 20 mV s^{-1} of them were highly similar to that of δ-($Na^+{}_yMn^{3+}{}_yMn^{4+}{}_{1-y}$)$O^{2-}{}_2$@ACC, demonstrating that their charge storage process of these electrodes include the surface capacitive and the diffusion-controlled processes (Supplementary Fig. 4a). The areal capacitances (Supplementary Fig. 4c) are determined from the GCD curves (Supplementary Fig. 4b), while the rate capabilities (Supplementary Fig. 4f) are calculated based on the capacitance retentions upon increasing the discharge current density from 5 to 30 mA cm^{-2} (Supplementary Fig. 4c).

Upon increasing electrolyte concentration for *in-situ* inserting Li^+ shutter ions from 0.5 to 1.5 M, the areal capacitances at 5 mA cm^{-2} of δ-$(Li^+{}_yMn^{3+}{}_yMn^{4+}{}_{1-y})O^{2-}{}_2$@ACC electrodes are elevated from 3286 to 4220 mF cm^{-2}, and the rate capabilities are boosted from 40.02% to 55.78%, respectively. Moreover, the capacitance retentions of δ-$(Li^+{}_yMn^{3+}{}_yMn^{4+}{}_{1-y})O^{2-}{}_2$@ACC after charge/discharge at 30 mA cm^{-2} of 10,000 cycles decrease from 19% to 9%, being much lower than that of ε-MnO_2@ACC (51%, Supplementary Fig. 4d). The R_s values of δ-$(Li^+{}_yMn^{3+}{}_yMn^{4+}{}_{1-y})O^{2-}{}_2$@ACC stepwise increase from 4.77 to 5.04 Ω, which are higher than that of ε-MnO_2@ACC (4.30 Ω) (Supplementary Fig. 4e-f). The above comprehensive analysis demonstrates that the optimal electrolyte concentration for *in-situ* inserting Li^+ shutter ions into ε-MnO_2@ACC is 1.5 M Li_2SO_4, which can significantly boost areal capacitance and rate capability, but significantly decrease cycle stability and increase R_s values. The higher supercapacitive performance of δ-$(Na^+{}_yMn^{3+}{}_yMn^{4+}{}_{1-y})O^{2-}{}_2$@ACC electrode compared to that of δ-$(Li^+{}_yMn^{3+}{}_yMn^{4+}{}_{1-y})O^{2-}{}_2$@ACC primarily attributed to the better matching of Na^+ hydrated diameter (7.1 Å) with the interlayer distance of δ-MnO_2 (7.0 Å), and the higher surface areas of δ-$(Na^+{}_yMn^{3+}{}_yMn^{4+}{}_{1-y})O^{2-}{}_2$@ACC during charge/discharge cycling.

6.0 PXRD pattern of Fe_2O_3@ACC

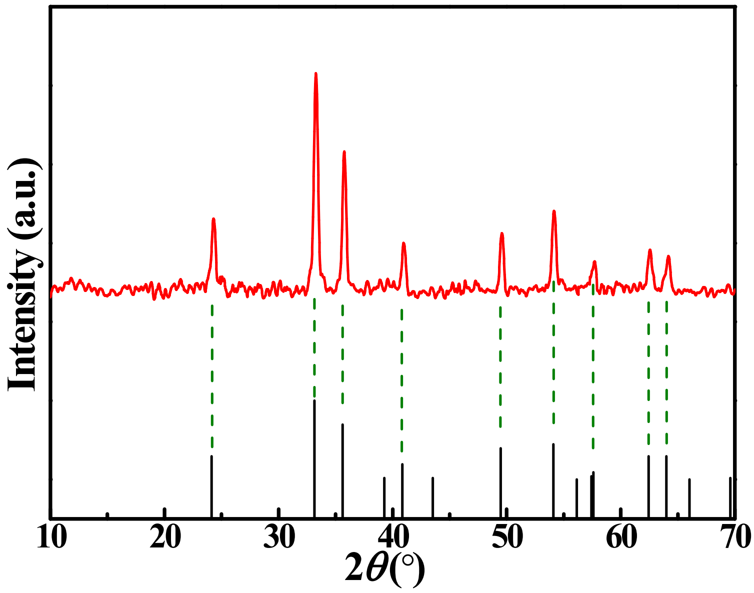

Supplementary Fig. 5 The measured PXRD pattern of as-synthesized Fe_2O_3@ACC and the PXRD pattern of Fe_2O_3 (PDF # 33-0664) obtained from the powder diffraction file (PDF). Note: the interference peaks from the ACC are subtracted in the measured PXRD for clarity.

Since the negative electrode also plays a critical role in the electrochemical performance of final fabricated asymmetric supercapacitor, Fe_2O_3 *in situ* grown on ACC (Fe_2O_3@ACC) with high areal capacitances is selected as anode. All peaks in the PXRD of Fe_2O_3@ACC match well with the rhombohedral Fe_2O_3 (PDF # 33-0664), indicating that the successful synthesis of rhombohedral Fe_2O_3 with high purity and crystallinity (**Supplementary Fig. 5**).[3]

7.0 Electrochemical performance of Fe_2O_3@ACC

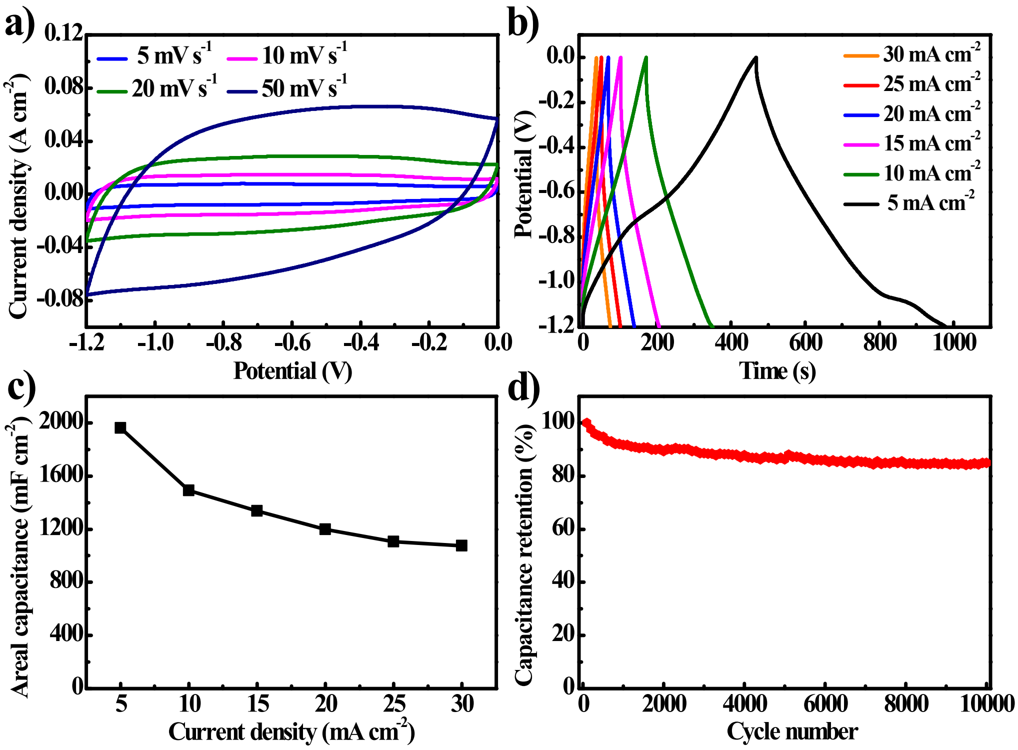

Supplementary Fig. 6 Electrochemical performance of Fe_2O_3@ACC tested in 1.5 M Na_2SO_4: (a) CV curves at different scan rates ranging from 5 to 50 mV s^{-1}, (b) GCD curves at different discharge current densities ranging from 5 to 30 mA cm^{-2}, (c) the areal capacitances at various discharge current densities ranging from 5 to 30 mA cm^{-2}, (d) the plots of areal capacitance at 30 mA cm^{-2} over 10,000 charge/discharge cycles.

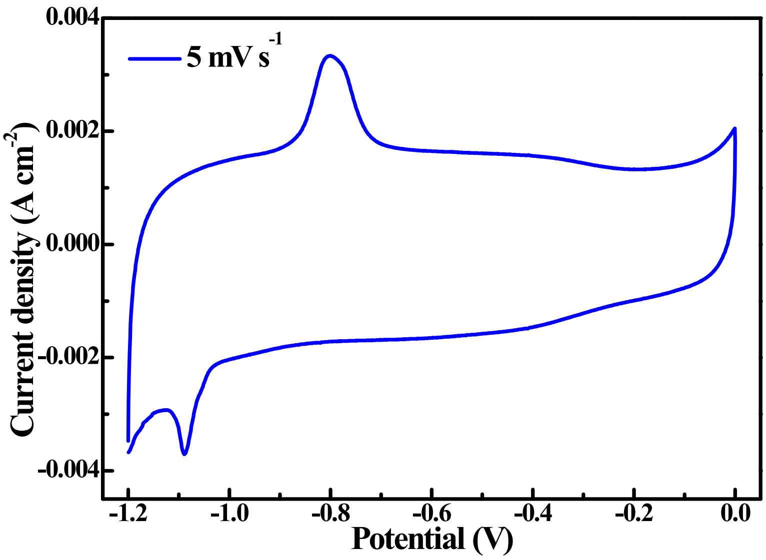

Supplementary Fig. 7 The enlarged CV curve of Fe_2O_3@ACC at a scan rate of 5 mV s^{-1}.

To meet the requirements of the energy density on the industrial level, we planned to construct asymmetric supercapacitors to extend voltage and increase the energy density of the energy storage device, besides the fabrication of δ-($Na^{+}_{0.48}Mn^{3+}_{0.48}Mn^{4+}_{0.52}$)$O^{2-}_{2}$@ACC positive electrodes with high electrochemical performances. Here, the Fe_2O_3 *in-situ* growing on ACC is fabricated as negative electrode, and the recorded CV curves of Fe_2O_3@ACC (Supplementary Fig. 6a) at different scan rates is approximal rectangular, illuminating that the areal capacitance of Fe_2O_3@ACC are primarily contributed from electric double layer capacitance (EDLC). Noticeably, the enlarged CV curve of Fe_2O_3@ACC at a scan rate of 5 mV s^{-1} exhibits a clear redox peak, demonstrating that pseudocapacitive behavior is also contributed to the high capacitance of Fe_2O_3@ACC (Supplementary Fig. 7). The appearance of significant plateaus in GCD curve at 5 mA cm^{-2} further demonstrate that the high areal capacitance of Fe_2O_3@ACC is composed of both EDLC and pseudocapacitance (Supplementary Fig. 6b).[4] The areal capacitance at 5 mA cm^{-2} of Fe_2O_3@ACC is high up to 1960 mF cm^{-2} (Supplementary Fig. 6b-c). Furthermore, Fe_2O_3@ACC possesses a good rate capability of 54.8% upon increasing current densities from 5 to 30 mA cm^{-2} and excellent capacitance retention of 85% after 10,000 charge/discharge cycles at 30 mA cm^{-2} (Supplementary Fig. 6d). These above results demonstrate that Fe_2O_3@ACC exhibits excellent electrochemical performance, and can be selected as the negative electrode material for assembling of asymmetric supercapacitors, in which δ-($Na^{+}_{0.48}Mn^{3+}_{0.48}Mn^{4+}_{0.52}$)$O^{2-}_{2}$@ACC is used as positive electrodes.

8.0 Electrochemical performance of δ-($M^+{}_yMn^{3+}{}_yMn^{4+}{}_{1-y}$)$O^{2-}{}_2$@ACC ($M^+$= Rb^+, Cs^+)

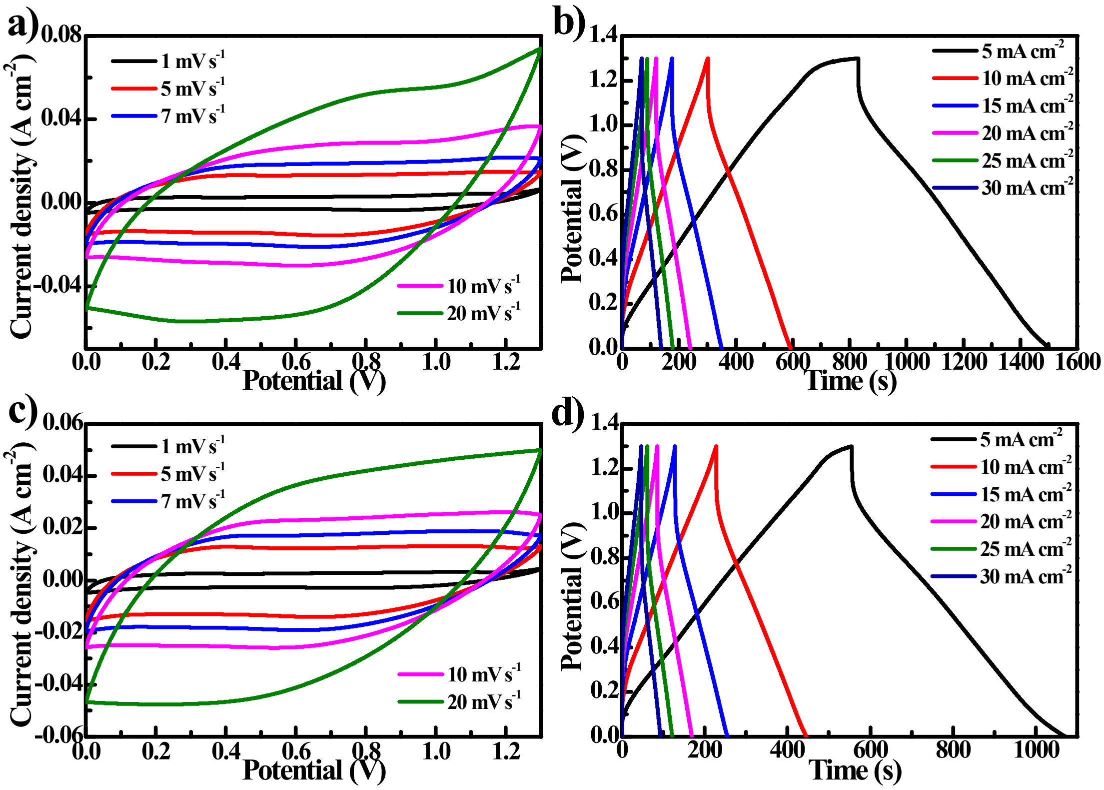

Supplementary Fig. 8 Electrochemical performances of δ-($M^+{}_yMn^{3+}{}_yMn^{4+}{}_{1-y}$)$O^{2-}{}_2$@ACC ($M^+$= Rb^+, Cs^+), in which M^+ was inserted by CV sweep at 1.5 M Rb_2SO_4 and 4.5 M Cs_2SO_4 electrolyte, respectively, for 500 times: (a) CV curves at different scan rates ranging from 1 to 20 mV s^{-1} of δ-($Rb^+{}_yMn^{3+}{}_yMn^{4+}{}_{1-y}$)$O^{2-}{}_2$@ACC, (b) GCD curves at different discharge current densities ranging from 5 to 30 mA cm^{-2} of δ-($Rb^+{}_yMn^{3+}{}_yMn^{4+}{}_{1-y}$)$O^{2-}{}_2$@ACC, (c) CV curves at different scan rates ranging from 1 to 20 mV s^{-1} of δ-($Cs^+{}_yMn^{3+}{}_yMn^{4+}{}_{1-y}$)$O^{2-}{}_2$@ACC, (d) GCD curves at different discharge current densities ranging from 5 to 30 mA cm^{-2} of δ-($Cs^+{}_yMn^{3+}{}_yMn^{4+}{}_{1-y}$)$O^{2-}{}_2$@ACC. Note: The electrochemical performances of δ-($Rb^+{}_yMn^{3+}{}_yMn^{4+}{}_{1-y}$)$O^{2-}{}_2$@ACC and δ-($Cs^+{}_yMn^{3+}{}_yMn^{4+}{}_{1-y}$)$O^{2-}{}_2$@ACC were tested in 1.5 M Rb_2SO_4 and 1.5 M Cs_2SO_4, respectively.

In order to further investigate the size effect of inserted shutter alkali metal ions with ionic diameter larger than K^+ on the electrochemical performances of ε-MnO_2 based electrodes, the δ-($M^+{}_yMn^{3+}{}_yMn^{4+}{}_{1-y}$)$O^{2-}{}_2$@ACC ($M^+$= Rb^+, Cs^+) electrodes were synthesized by the CV sweep method, being similar to that of the δ-($Na^+{}_{0.48}Mn^{3+}{}_{0.48}Mn^{4+}{}_{0.52}$)$O^{2-}{}_2$@ACC electrode. The disparity between these synthesis methods is only replacing 1.5 M Na_2SO_4 with the saturated electrolyte 1.5 M Rb_2SO_4 and 4.5 M Cs_2SO_4, respectively. The shape of CV curves at the scan rate ranging from 1 to 20 mV s^{-1}

of δ-($M^{+}_{y}Mn^{3+}_{y}Mn^{4+}_{1-y}$)$O^{2-}_{2}$@ACC ($M^{+}$= Rb^{+}, Cs^{+}) were highly similar to that of δ-($Na^{+}_{y}Mn^{3+}_{y}Mn^{4+}_{1-y}$)$O^{2-}_{2}$@ACC, demonstrating that the charge storage processes of these two electrodes are similar to that of δ-($Na^{+}_{y}Mn^{3+}_{y}Mn^{4+}_{1-y}$)$O^{2-}_{2}$@ACC, including the surface capacitive and the diffusion-controlled processes (Supplementary Fig. 8a, c). The areal capacitance at 5 mA cm^{-2} of δ-($Rb^{+}_{y}Mn^{3+}_{y}Mn^{4+}_{1-y}$)$O^{2-}_{2}$@ACC and δ-($Cs^{+}_{y}Mn^{3+}_{y}Mn^{4+}_{1-y}$)$O^{2-}_{2}$@ACC, determined from the GCD curves, are 2584 and 1980 mF cm^{-2}, respectively, being much lower than that of ε-MnO_2@ACC (4192 mF cm^{-2}) and δ-($Na^{+}_{0.48}Mn^{3+}_{0.48}Mn^{4+}_{0.52}$)$O^{2-}_{2}$@ACC (5875 mF cm^{-2}). The rate capability of them, calculated from the capacitance retention upon increasing the discharge current density from 5 to 30 mA cm^{-2} (Supplementary Fig. 8b, d) are 61.6% and 53.6%, respectively, being much lower than that of δ-($Na^{+}_{0.48}Mn^{3+}_{0.48}Mn^{4+}_{0.52}$)$O^{2-}_{2}$@ACC (77.8%), but higher than ε-MnO_2@ACC (41.3%). These results demonstrate that the better matching of M^{+} hydrated diameter with the interlayer distance of δ-MnO_2 (7.0 Å) leads to the higher cycle stability of δ-($M^{+}_{y}Mn^{3+}_{y}Mn^{4+}_{y}$)$O^{2-}_{2}$@ACC electrode.

9.0 Supplementary References

1 Y. Fu, Y. J. Gu, Y. B. Chen, H. Q. Liu and H. H. Zhou, *Solid State Ionics*, 2018, **320**, 16-23.

2 Q. L. Ye, R. T. Dong, Z. H. Xia, G. R. Chen, H. L. Wang, G. J. Tan, L. Jiang and F. Wang, *Electrochim. Acta*, 2014, **141**, 286-293.

3 J. Li, Y. W. Wang, W. N. Xu, Y. Wang, B. Zhang, S. Luo, X. Y. Zhou, C. L. Zhang, X. Gu and C. G. Hu, *Nano Energy*, 2019, **57**, 379-387.

4 Y. Jiang and J. Liu, *Energy Environ. Mater.*, 2019, **2**, 30-37.